ACS APPLIED MATERIALS & INTERFACES

Research Article

www.acsami.org

Tuning Morphology of Nanostructured ZIF-8 on Silica Microspheres and Applications in Liquid Chromatography and Dye Degradation

Adham Ahmed,[†] Mark Forster,[†] Junsu Jin,[‡] Peter Myers,[†] and Haifei Zhang*[,†]

[†]Department of Chemistry, University of Liverpool, Liverpool L69 7ZD, United Kingdom

[‡]Beijing Key Laboratory of Membrane Science and Technology, College of Chemical Engineering, Beijing University of Chemical Technology, Beijing 100029, China

Supporting Information

ABSTRACT: Zeolitic imidazolate framework-8 (ZIF-8) is one type of metal−organic framework (MOF) with excellent thermal and solvent stability and has been used extensively in separation, catalysis, and gas storage. Supported ZIF-8 structures can offer additional advantages beyond the MOF-only materials. Here, spheres-on-spheres (SOS) silica microspheres are used as support for the nucleation and growth of ZIF-8 nanocrystals. The surface functionalities (−SH, −COOH, and $-NH_2$) of silica and reaction conditions are investigated for their effects on the ZIF-8 morphology. The use of SOS microspheres results in the formation of highly crystalline ZIF-8 nanostructured shell with varied sizes and shapes, ranging from spherical to cubic and to needle crystals. The SOS@ZIF-8 microspheres are packed into a column and utilized for separation of aromatic molecules on the basis of $\pi-\pi$ interaction in high-performance liquid chromatography (HPLC). Furthermore, by thermal treatment in air, ZIF-8 nanocrystals can be transformed into ZnO coating on SOS silica microspheres. The SOS@ZnO microspheres show excellent photocatalytic activity, as measured by degradation of methyl orange in water, when compared to ZnO nanoparticles. This study has demonstrated the facile way of using SOS microspheres to prepare core−shell microspheres and their applications.

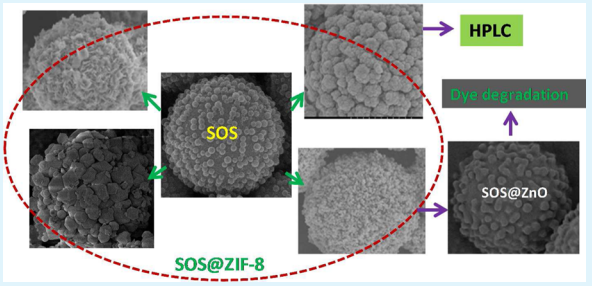

KEYWORDS: *silica microspheres, ZIF-8, metal−organic frameworks, HPLC, dye degradation*

INTRODUCTION

Research into the area of porous materials has been of great interest because of their wide range of applications such as in drug delivery,[1] separation,[2] and catalysis.[3] Highly ordered, crystalline porous materials such as metal−organic frameworks (MOFs) exhibit unique advantages for these applications.[4] Zeolitic imidazolate frameworks (ZIFs) are a subclass of MOFs that have attracted great attention because they combine the desirable properties of both zeolites and MOFs such as microporosity, crystallinity, high surface area, and high chemical and thermal stability.[4,5] Different ZIFs have been synthesized, usually employing a metal ion (e.g., zinc or cobalt) coordinated through nitrogen to imidazolate linkers to form a neutral framework with tunable nanopores. The pores are formed by the presence of ZnN_4 tetrahedral clusters, and their pores and channels allow access of guest molecules for applications such as gas storage and catalysis.[5,6]

Similar to most MOFs, ZIF-8 can be synthesized by a solvothermal method.[6] ZIF-8 can also be prepared at room temperature in solvents including methanol and water when an excess amount of the ligand 2-methyl imidazole (2-MeIM) is used.[7,8] This can be achieved simply by mixing the starting materials in solution (e.g., zinc nitrate and 2-MeIM) without even stirring the solution. The reaction times can be much shorter, taking only minutes compared to hours/days for solvothermal methods.[4−8] Controlling the crystal size and shape of ZIF-8 may be done by modulating the rate of nucleation and growth or via the approach of cooling-induced crystals.[9,10] Cravillon et al. showed that ZIF-8 crystalline particles could be formed at room temperature in sizes ranging from 10 nm to 1 μm by using auxiliary monodentate ligands in addition to the excess amount of the bridging bidentate ligand 2-MeIM.[9] By rapid cooling of the reaction system, spherical agglomerates, rhombic dodecahedron, or truncated rhombic dodecahedron particles could be produced depending on the initial heating temperature.[10] The influence of various solvents (aliphatic alcohols, water, dimethylformamide, and acetone) was investigated for the synthesis of ZIF-8 nanocrystals at room temperature. The solvent hydrogen bond donation ability seemed to be the main factor over ZIF-8 crystallization.[11] For water-based synthesis, a variety of zinc salts were systematically studied without any additives at room temperature. It was found that the morphology of ZIF-8 nanocrystals was considerably impacted by ligand concentration, ratio of ligand to Zn^{2+}, and water content.[12] The crystal morphology transformation occurred in solution during the synthesis of

Received: June 5, 2015
Accepted: July 23, 2015
Published: July 23, 2015

DOI: 10.1021/acsami.5b04979
ACS Appl. Mater. Interfaces 2015, 7, 18054−18063

ZIF-8. It was possible to monitor the morphology transformation of ZIF-8 particles from metastable amorphous phase to nucleation and growth to a crystalline phase.[13]

Enormous effort has been paid to form ZIF-8 thin films or coatings on particles/nanowires for separation (e.g., as stationary phase[14] or membrane).[15] Surface functionality is critical for ZIF growth in order to improve adherence and coverage on the scaffold. ZIF-8 synthesis/deposition on different supports such as polymer,[16] alumina,[17] and silica[14,18] have been demonstrated. By manipulating the growth kinetics through change of anion, solvent, and reaction time, it was possible to produce orientated ZIF-8 membrane with sharp H_2/C_3H_8 separation.[19] The thickness of ZIF-8 shell on silica spheres may be controlled via repetitive coating cycles.[14,18] A number of studies have been carried out to utilize MOFs in analytical chemistry in order to address the challenges in analysis sensitivity and selectivity. MOFs can be either directly packed into a column or ground into smaller crystals before packing.[20−22] The low packing efficiency and crushing of MOF particles under operational pressure can reduce column efficiency and reproducibility and also irreversibly increase back pressure. This issue may be overcome with the use of solid spherical supports for the growth of MOF crystals such as ZIF-8.[14,18]

The textile, leather, and paper manufacturing industries involve extensive use of various dyes that can be introduced into the aquatic systems and thus cause environmental pollution and health hazards.[23] Dye remediation has been investigated/carried out by various methods such as adsorption, biological means, and chemical degradation methods.[23−27] Photocatalytic degradation of organic pollutants in water has attracted much attention in recent years.[26−28] Various nanostructured metal oxides, particularly TiO_2, have been used as catalysts for photodegradation.[25,28,29] Recently, ZnO has emerged as a promising heterogeneous catalyst for wastewater treatment because of its wide band gap of 3.37 eV and a large exciton binding energy of 60 meV.[30−33] ZnO particles could be synthesized by chemical synthesis or thermal decomposition (e.g., from zinc oxalate).[31−33] ZIF-8 was thermally treated in air (500 °C) to produce porous ZnO particle or hollow hybrid nanostructures for catalytic reactions.[34,35] ZnO nanostructures may provide excellent degradation performance, but the removal and reusability of such nanoparticles from aqueous phase are important issues, particularly for large scale applications.[25,28] ZIF-8 nanocrystals were prepared on 3D grapheme networks (3DGN). After thermal annealing at 450 °C under Ar and thermal treatment in air at 380 °C, ZnO/3DGN was formed and demonstrated superior performance for methylene blue degradation over that achieved by ZnO prepared from ZIF-8.[36] However, reports of coating ZnO on silica spheres for photodegradation of organic pollutants are rare. Not only can the silica microspheres facilitate catalyst collection and recycling, but also the composite spheres can be packed efficiently in a column/reactor for potentially continuous wastewater treatment.

Herein, we use the recently developed spheres-on-sphere (SOS) silica as support for the growth of ZIF-8 nanocrystals. SOS silica can be synthesized from (3-mercaptopropyl)trimethoxysilane using a modified Stöber method, where silica nanospheres are formed on the silica microspheres in a one-pot synthesis procedure at room temperature.[37] The silica microspheres are nonporous, but the assembled nanospheres on the microspheres can provide interstitial porosity for fast separation of small and large molecules.[38,39] The surface functionalities of the SOS particles may be readily modified via silane chemistry for improved separation or further formation/attachment of other types of nanocrystals.[14,38,40] In this study, the influence of surface functionality (−SH, $-NH_2$, and −COOH) on the ZIF-8 crystal growth on the SOS surface is studied. Core−shell SOS@ZIF-8 spheres are evaluated as stationary phase for chromatographic separation of aromatic molecules by HPLC. Furthermore, SOS@ZIF-8 spheres are thermally treated to generate SOS@ZnO spheres that are utilized as catalyst for the photodegradation of methyl orange.

EXPERIMENTAL SECTION

Chemicals and Reagents. (3-Mercaptopropyl)trimethoxysilane (MPTMS, 95%), cetyltrimethylammonium bromide (CTAB, ≥ 98%), 3-aminopropyl triethoxysilane (APTES, ≥ 98%), 2-methylimidazole (2-MeIM, 95%, M_w = 82.10), pyridine (≥99.0%), HCl solution, ammonium hydroxide solution (reagent-grade, 28−30% NH_3 basis), poly(vinyl alcohol) (PVA, M_w = 10 000), zinc nitrate hexahydrate ($Zn(NO_3)_2{\cdot}6H_2O$, M_w = 279.49), and all solvents were purchased from Sigma-Aldrich and used as received. HPLC-grade solvents were used for HPLC tests.

Preparation of SOS Silica Particles. A previously reported procedure was followed.[37] Typically, PVA (0.25 g) and CTAB (0.1 g) were dissolved in 5 g of water. To this solution, 8 mL of methanol was added while stirring. As-purchased ammonium hydroxide solution was diluted with water to 5.6%, and 2 mL of this solution was added into the reaction mixture. After stirring for 15 min, 0.5 mL of MPTMS was added dropwise over a 30 s period. The reaction was stirred for 24 h at room temperature. The resulting silica microspheres were collected by centrifugation at 3000 rpm for 3 min (Eppendorf centrifuge 5415D). As a control, smooth silica spheres were prepared using the same procedure except that no CTAB was added. The as-prepared SOS particles were coded as SOS-SH because of the presence of −SH groups. The modification of the SOS particles with $-NH_2$ and −COOH was carried out by the same procedures reported previously.[40]

Synthesis of SOS@ZIF-8 Microspheres. Synthesis of ZIF-8 was carried out in the presence of SOS spheres using water or methanol as solvent. In each procedure, the stock solutions of $Zn(NO_3)_2$ and 2-MeIM with the same solvent were used.

Procedure 1. Stock solutions of $Zn(NO_3)_2{\cdot}6H_2O$ (0.117 g) in 0.8 g of water (or methanol) and 2-MeIM (2.270 g) in 8 g of water (or methanol) were prepared. The molar ratio of $Zn(NO_3)_2$ to 2-MeIM when the two stock solutions were mixed together was 1:66:1147 (H_2O) or 1:66:644 (MeOH).

Procedure 2. Stock solutions of $Zn(NO_3)_2{\cdot}6H_2O$ (0.058 g) in 0.8 g of water and 2-MeIM (0.129 g) in 8 g of water were prepared. The molar ratio of $Zn(NO_3)_2$ to 2-MeIM when the two stock solutions were mixed together was 1:7.4:2313 (H_2O) or 1:7.4:1301 (MeOH).

Zn^{2+} ions were immobilized by mixing 0.05 g of SOS particles with the prepared $Zn(NO_3)_2$ stock solution. After stirring with magnetic bar for 1 h, 2-MeIM stock solution was added. The resulting suspension was stirred for 1 h and then allowed to age for 24 h at room temperature. The produced SOS@ZIF-8 particles were precipitated from the suspension by centrifugation at 1000 rpm for 5 min. After removing the supernatant phase, fresh methanol (10 mL) was added to the SOS@ZIF-8 particles. The resulting suspension was centrifuged again at 1000 rpm for 5 min. This procedure was repeated three times to ensure the complete removal of unattached MOF from the composite particles.

Column Packing and HPLC Assessment. SOS-COOH@ZIF-8 particles prepared via procedure 2 with methanol were selected for HPLC assessment because of the dense coating on silica surface. Multiple batches of the microspheres were prepared and mixed together. To pack the column, SOS-COOH@ZIF-8 particles (1 g) were suspended in 15 mL of methanol/chloroform (75:25 v/v%) by ultrasonication for 30 min (sonication bath, Fisherbrand FB11021). The slurry was poured into a 15 mL reservoir and packed into a 3 mm

DOI: 10.1021/acsami.5b04979
ACS Appl. Mater. Interfaces 2015, 7, 18054−18063

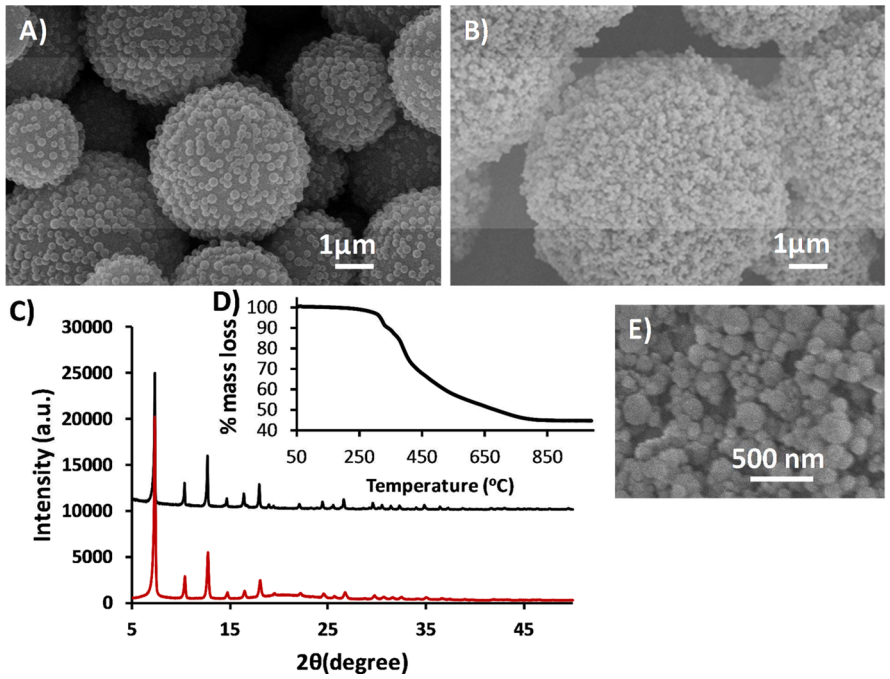

Figure 1. (A) The SEM image of the as-prepared SOS-SH particles before modification. (B) SEM image of SOS-SH@ZIF-8 particles prepared by procedure 1 in H_2O. (C) PXRD patterns of ZIF-8 (black line) and SOS-SH@ZIF-8 particles (red line). (D) TGA curve of the SOS-SH@ZIF-8 particles. (E) Image with high magnification showing the surface feature of the SOS-SH@ZIF-8 particles.

(I.D.) × 100 mm (L) stainless steel column using the in-house packing method at 350 bar with Knauer K-1900. The column was activated by heating at 150 °C for 3 days and then flushed with methanol before testing.

For the HPLC tests, the column was fitted into an Agilent 1200 series HPLC, comprising a vacuum degasser, quaternary pump, ALS autosampler, heated column compartment, and a UV−vis detector. All the tests were carried out at 20 °C unless otherwise stated. All signals were UV-detected at 254 nm. Data analysis was carried out using Agilent Chemstation software, version B.02.01 (Agilent Technologies, USA). The plate numbers were calculated by the equation $N = 5.54(t_R/W_{1/2})^2$, where t_R is the retention time and $W_{1/2}$ is the half-height peak width of the peak concerned.

Photodegradation of Methyl Orange. SOS-SH@ZIF-8 particles were heated to 550 °C in air for 2 h to form SOS@ZnO particles. SOS@ZnO particles (120 mg/L) were added into aqueous methyl orange solution (10 mg/L). The degradation was initiated using a 40 W UV lamp light at 365 nm with stirring. (The distance from the solution level to the UV lamp was determined to be around 10 cm.) The change of methyl orange concentration was monitored by UV−vis spectrophotometer. A 900 μL aliquot of liquid was taken from the methyl orange solution and centrifuged for 10 min at 1000 rpm to obtain a clear solution. A 300 μL aliquot of the clear solution was used for UV−vis analysis at 460 nm. All the solution and the precipitated particles were then placed back into the original solution to continue the degradation reaction.

Characterization. The morphologies were observed by a Hitachi S-4800 scanning electron microscope (SEM) equipped with an EDX detector. One drop of the suspension in ethanol was deposited on an SEM stud and allowed to dry overnight. The samples were then coated with gold using a sputter coater (EMITECH K550X) for 2 min at 25 mA before imaging. The Brunauer−Emmett−Teller (BET) surface area and pore size distribution by N_2 sorption at 77 K were measured using a Micromeritics ASAP 2420 adsorption analyzer. The micropore size distributions were calculated by the nonlocal density functional theory (NLDFT) method that is suitable for micropores. Samples were degassed for 10 h at 120 °C before N_2 sorption analysis. Powder X-ray diffraction (PXRD) data were collected on a Panalytical X'Pert Pro Multi-Purpose Diffractometer in high-throughput transmission geometry. The Cu anode operated at 40 kV and 40 mA. Samples were pressed into the well of an aluminum plate. The PXRD patterns were collected over 5−50° 2θ with a scan time of 40 min. The microspheres were also characterized by high-throughput Fourier transform infrared spectroscopy (FTIR, model Tensor 27, HTS-XT, Bruker). The inductively coupled plasma (ICP) microanalysis was conducted on a Specto Ciros Charged Coupled Device using ICP-optical emission spectrometry-side on plasma. The photodegradation of methyl orange was measured using a UV plate reader (μQuant, Bio-Tek Instruments, Inc.) and an acrylic 96-well plate. Thermal stability of the materials was investigated by thermal gravimetric analysis (TGA, Model Q5000IR TGA, TA Instruments).

RESULTS AND DISCUSSION

Synthesis of ZIF-8 on SOS-SH Microspheres. The SOS silica microspheres were prepared using MPTMS as precursor (Figure 1A). The SOS spheres have thiol groups on their surface that offer high affinity to a range of metal ions.[41,42] When SOS particles were mixed with $Zn(NO_3)_2$ solutions, the affinity of Zn^{2+} to −SH groups led to the adsorption of Zn^{2+} onto SOS particles, which could act as anchoring points for the formation and growth of ZIF-8 nanocrystals. ZIF-8 crystals could be synthesized in organic solvents and in water.[5−8,11,12] Organic solvents are not only expensive but also pose environmental risks such as toxicity and flammability. It was possible to promote crystal growth in aqueous solutions by using high concentrations of 2-MeIM.[8,12] Here, we first attempted synthesis of ZIF-8 crystals onto SOS particles in aqueous medium with a high ratio of 2-MeIM to Zn^{2+} (procedure 1 with water). SEM imaging of the obtained material showed that the SOS microspheres were covered with nanoparticles around ∼50 nm in diameter (Figure 1B). The crystallinity of this material was confirmed (Figure 1C) and consistent with the PXRD pattern of the commonly synthesized ZIF-8 crystals.[5−8] The PXRD pattern showed sharp and high intensity peaks, demonstrating that highly pure

DOI: 10.1021/acsami.5b04979
ACS Appl. Mater. Interfaces 2015, 7, 18054−18063

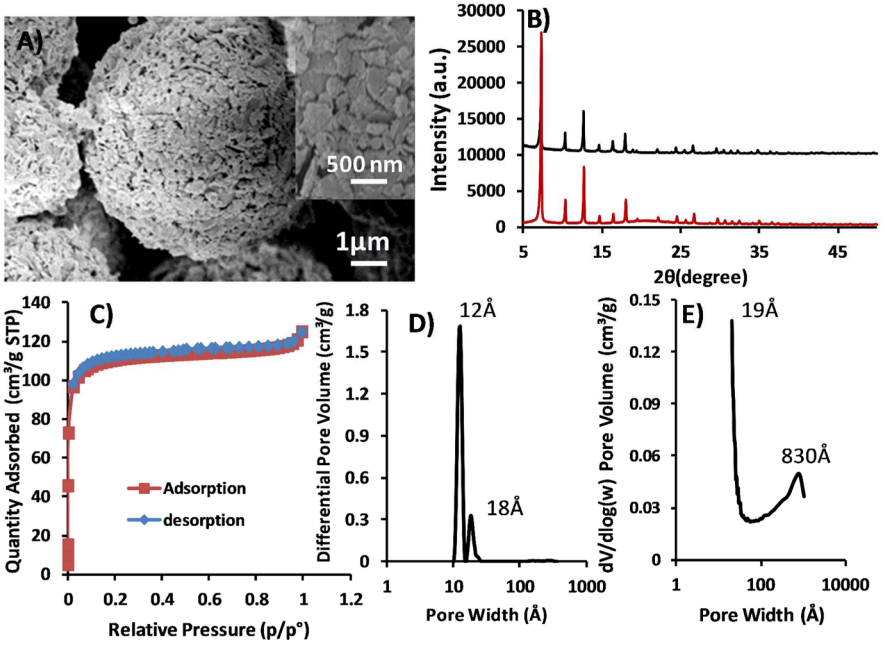

Figure 2. (A) SEM image of the SOS-SH@ZIF-8 (procedure 2/H_2O) and close look of the porous shell morphology (insert). (B) PXRD patterns of the ZIF-8 nanocrystals (black line) and the SOS-SH@ZIF-8 microspheres (red line). (C) Nitrogen adsorption−desorption isotherm of the composite microspheres at 77 K. (D) Microspore size distribution obtained using the NLDFT method. (E) BJH pore size distribution calculated from the adsorption branch of the isotherm.

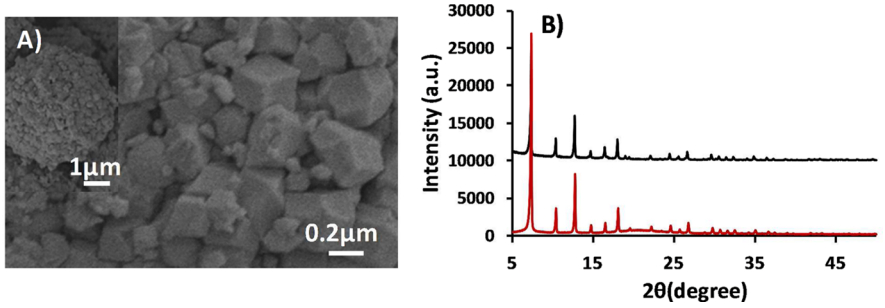

Figure 3. (A) Shell morphology of SOS-SH@ZIF-8 prepared by procedure 2 with methanol as solvent. (B) PXRD patterns of the ZIF-8 nanocrystals (black line) and the prepared SOS-SH@ZIF-8 composite microspheres (red line).

ZIF-8 nanocrystals were formed. The TGA analysis in air at 1000 °C (Figure 1D) showed the inorganic component of 44.48% (SiO_2 + ZnO), 5.28% higher than the inorganic component of SOS particles only.[40] The surface coverage of ZIF-8 nanocrystals was quite uniform. It appeared that the nanocrystals were prone to growing onto the silica nanospheres and not densely covering the whole surface, probably because of the easy access to the silica nanosphere active sites (Figure 1E). It should be mentioned that the description of uniform or densely growing ZIF-8 nanocrystals is based on the SEM imaging and comparison of the SOS@ZIF-8 composite microspheres prepared in this study.

The reaction conditions were varied (i.e., the precursor concentration and the ratio of Zn^{2+} to 2-MeIM) to tune the morphology of ZIF-8 crystals. A high concentration of the ligand was needed to form ZIF-8 crystals in the previous studies.[7,8,12] Here, with synthesis by procedure 2 in water, ZIF-8 nanoplates coating SOS particles were observed (Figure 2A). These ZIF-8 nanoplates with sizes up to 250 nm were densely grown in between the silica nanospheres on the silica surface. This was significantly different from the SOS@ZIF-8 particles prepared by procedure 1, where mainly ZIF-8 nanoparticles of around 50 nm were formed on the surface (Figure 1B).

The PXRD pattern again confirmed the crystalline phase of the ZIF-8 coating (Figure 2B). Nitrogen sorption measurement of the SOS-SH@ZIF-8 particles at 77K revealed a type-I isotherm, indicating a highly microporous material (Figure 2C). This resulted from the ZIF-8 coating because the as-prepared SOS-SH particles were nonporous.[37] The apparent BET surface area of the composite microspheres was 495 m^2/g with pore volume of 0.19 mL/g. Total N_2 uptake of 124 mL/g at a relative pressure p/p^0 = 0.95 is 31% of that observed for the pure bulk ZIF-8 (400 mL/g).[43] The pore size distribution calculated using NLDFT method showed micropores peaked at 1.2 nm (or 12 Å, consistent with the pore cage diameter)[6,12] and 1.8 nm (or 18 Å, Figure 2D). A slight hysteresis was observed upon desorption, which revealed mesopores around 83 nm on the basis of Barrett−Joyner−Halenda (BJH) calculation (mesopore volume = 0.0154 mL/g). These mesopores and the additional macropores (>50 nm) compared to ZIF-8 are believed to be from the interstices of aggregated particles in the material. The TGA data showed an inorganic component of 45.07% at 1000 °C (Figure S1).

DOI: 10.1021/acsami.5b04979
ACS Appl. Mater. Interfaces 2015, 7, 18054−18063

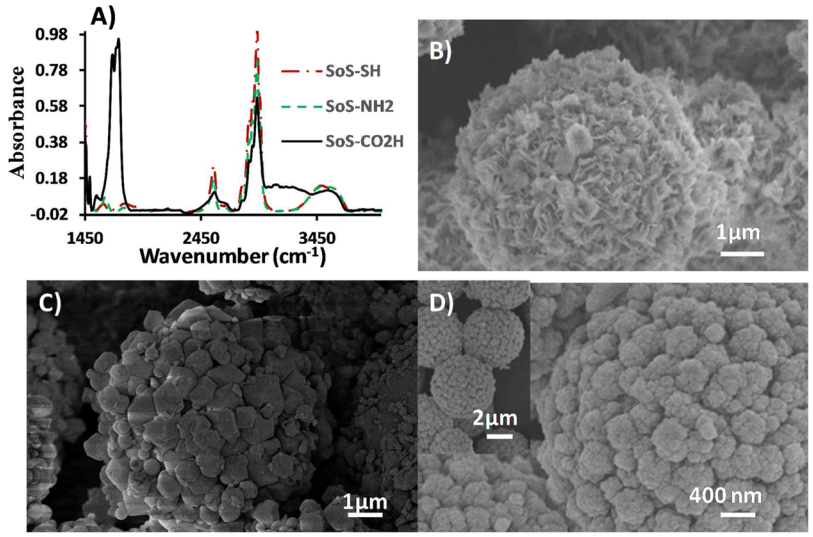

Figure 4. (a) FTIR spectra of SOS particles modified with different surface groups. Influence of surface functionality on ZIF-8 crystal morphology: (B) SOS-NH_2 with procedure 2 in H_2O, (C) SOS-NH_2 with procedure 2 in methanol, and (D) SOS-COOH with procedure 2 in methanol.

Solvents can play an important role in controlling the crystal morphology because the rate of the crystal growth and mass transport can be altered by the movement and depletion of ions and molecules that feed the growing crystals at the crystal/solution interface in different solvents.[44] When the depletion zone is altered around the crystal, this affects the final crystal morphology. Water promotes faster rate of depletion for the Zn ions, whereas methanol offers a much slower rate of depletion. Thus, with methanol as solvent instead of water (procedure 2), large ZIF-8 crystals with a size up to 250 nm were formed on the SOS-SH sphere, and aggregation was observed in some areas (Figure 3A). The shape of the crystals changed from plates to cubiclike shapes because of the change in the crystal growth kinetics caused by solvent change (from water to methanol). The growth of large cubic-shaped ZIF-8 on solid supports was reported before, but a multiple-step procedure was required for a similar level of dense coating.[14,18] It is believed that the SOS particles offer a unique surface morphology that is favorable for ZIF-8 crystallization/growth. The concentration effect in the synthesis with methanol as solvent could be observed as well. For synthesis by procedure 1 in methanol, the ZIF-8 particles on SOS were spherical and sized in the nanometer range (25−50 nm) but with much less dense coating on silica surface (Figure S2). For both solvents, it seemed that the lower ratio of the ligand 2-MeIM to Zn^{2+} ions produced larger ZIF-8 crystals, whereas a higher ratio of 2-MeIM to Zn^{2+} resulted in ZIF-8 nanospheres on the SOS particles. The contribution from the concentration change is believed to be limited.[7−9]

Compared to the usual silica microspheres with smooth surface, the SOS particles provide a unique morphology of nanospheres covering the microspheres. The surface nanospheres can generate more external surface area and anchoring sites for further modification. To investigate how the silica surface morphology would influence the coating ZIF-8 nanocrystals morphology, a control study was carried out using the silica microspheres with smooth surface that were prepared without adding CTAB during the synthesis. A thick layer of ZIF-8 (hard-to-see individual particles) was formed on the surface of silica particles (Figure S3). The obtained shell morphology was significantly different, compared with that of the composite microspheres formed from the SOS particles (Figures S3 vs Figure 3A).

Modification of SOS Particles with $-NH_2$ and −COOH Groups for ZIF-8 Growth. The as-prepared SOS-SH particles were further chemically modified with −COOH and $-NH_2$ groups to produce a surface with bifunctional groups (−SH groups still present), which provided a different environment for ZIF-8 growth. The functional groups −COOH and −OH on silica have been shown to facilitate the coating of ZIF-8 crystals.[14,18] The $-NH_2$ groups may not greatly help to adsorb Zn^{2+} ions but may affect the growth of ZIF-8 crystals. FTIR analysis of dried particles confirmed the presence of $-NH_2$ and −COOH groups in addition to −SH groups on the SOS spheres (Figure 4A). The $-NH_2$ ligand showed vibration features similar to those of −SH ligand. Microanalysis results confirmed the presence of C (20.01%), H (5.31%), and N (0.25%), whereas the unmodified silica particles contained no nitrogen. In the case of −COOH ligand, one noticeable difference in the FTIR was the existence of strong peaks around 1710 and 1736 cm^{-1} caused by the presence of carbonyl and carboxylic acid groups, respectively. These functionalized SOS particles were used as scaffold for nucleation and growth of ZIF-8 on the surface.

Synthesis with modified SOS particles was first investigated in aqueous medium. Using procedure 1 and SOS-COOH particles, similar ZIF-8 shell morphology was observed (compared to that of the SOS-SH particles). The SOS-COOH particles were densely coated with ZIF-8 nanospheres. Interspacing porosity between the ZIF-8 nanospheres was estimated to be in the range of 50−100 nm on the basis of the SEM images (Figure S4). With procedure 2 in water, a thick ZIF-8 film covering the silica nanospheres on the surface of SOS particles was observed (Figure S5). Because both −COOH and −SH could adsorb Zn^{2+}, the effect of the presence of −COOH was not significant for the synthesis in aqueous medium. A distinct morphology change of ZIF-8 was observed when the SOS-NH_2 particles were used as the scaffold. Randomly packed nanoplate crystals were observed on the SOS surface when synthesis procedure 1 in water was followed (Figure S6). With synthesis by procedure 2, finer nanoplates were formed, appearing to grow from the SOS

DOI: 10.1021/acsami.5b04979
ACS Appl. Mater. Interfaces 2015, 7, 18054−18063

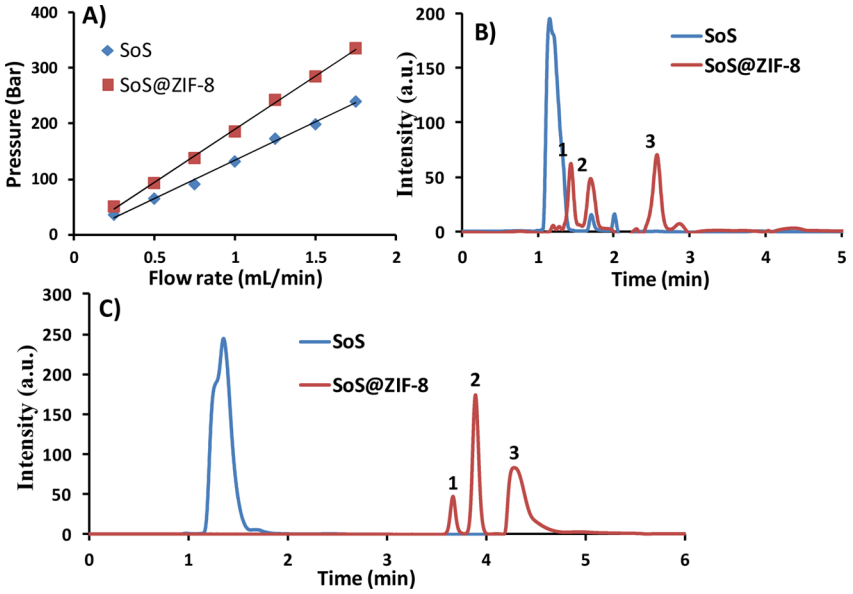

Figure 5. (A) Change of column back pressure generated from SOS-COOH particles and SOS-COOH@ZIF-8 particles at different flow rates using methanol/ethanediol 99.5:0.5 v/v% as mobile phase. (B) Chromatograms for the separation of (1) 1-(4-hydroxyl phenyl) ethanol, (2) 3-[1-(methyl amino) ethyl] phenol, and (3) 3-[1-(dimethyl amino) ethyl] phenol]. (C) Chromatograms for the separation of (1) phenol, (2) hydroquinone, and (3) bibenzyl-4,4′-diol. Both columns were tested under the same conditions: injection volume of 1 μL, mobile phase methanol/ethanediol 99.5:0.5 v/v% at a flow rate 0.35 mL/min, and test temperature of 20 °C.

surface (Figure 4B). The PXRD analysis demonstrated that the nanoplates were ZIF-8 crystals (Figure S7). It should be noted that the unattached ZIF-8 in suspension remained unchanged (Figure S8), which strongly suggests that the surface functional groups have a strong influence on the final morphology of ZIF-8 crystals. The BET surface areas are in the range of 250−400 m^2/g for the composite microspheres, varying depending on the different density of ZIF-8 coating on the surface under different synthesis conditions.

Similar to the use of SOS-SH particles, the morphology of the coating ZIF-8 crystals changed when methanol was used as solvent. Cubic-shaped crystals were mainly observed for the SOS-SH particles (Figure 3A). The noticeable morphology change was observed when the modified SOS particles were used for synthesis of ZIF-8 in methanol. With procedure 2 in methanol, large ZIF-8 crystals reaching up to 500 nm in diameter were formed on the SOS-NH_2 particles (Figure 4C). In the case of SOS-COOH particles, nanoaggregates were observed on the surface, which resembled the shape of the SOS morphology (Figure 4D). However, the change of the molar ratio of 2-MeIM to Zn^{2+} and the precursor concentration in methanol (procedure 1) had little impact on the final morphology of ZIF-8 nanocrystals. Similar morphologies were observed for SOS-NH_2@ZIF-8 particles (Figure S9 vs Figure 4C) and SOS-COOH@ZIF-8 particles (Figure S10 vs Figure. 4D).

The BET surface areas for the SOS@ZIF-8 composite particles are given in Table S1. Because the surface area for the SOS particles is very low (~3.5 m^2/g), the surface areas of the composite particles are indicative of the amount of ZIF-8 formed on the SOS surface. The surface area data suggest loading of ZIF-8 in the range of 11−42 wt %. From the SEM images obtained, ZIF-8 nanocrystals of varied sizes could form in the interstitial spaces between the silica nanospheres or grow onto the silica nanospheres on the SOS surface. It is difficult to accurately define the ZIF-8 thickness, but it is estimated to be in the range of 200−500 nm.

SOS@ZIF-8 for HPLC Separation of Aromatic Compounds. There have been a few studies on the use of ZIF-8 for liquid chromatography. Initial attempts included the packing of commercially available 4.9 μm ZIF-8 particles, but these resulted in poor separation efficiency, with a maximum theoretical plate of 81.91 for 3-(1-hydroxyphenyl)ethanol using a 5 cm long column, or 1638 plates/m.[22] The ZIF-8 separation efficiency was enhanced with the use of silica spheres as support, 23 000 plates/m achieved for bisphenol A.[14] However, in order to achieve the desirable separation, the particles underwent up to four cycles of ZIF-8 synthesis on silica microspheres.[14] The SOS@ZIF-8 composite microspheres prepared here represent a unique solid-core, porous-shell structure: the silica microsphere core is nonporous, whereas the shell consisting of dense ZIF-8 crystals entrapped between the silica nanospheres is porous. The SOS particles coated with HKUST-1 nanocrystals have demonstrated improved performance in column selectivity with the separation of xylene isomers. The xylene isomers could not be separated using the column packed with SOS only or HKUST-1 particles only.[40] ZIF-8 is significantly different from HKUST-1. Its chemical and thermal stability can offer greater opportunity for use in HPLC where different mobile phases are used to separate different types of analytes. It is therefore very important to assess the performance of the SOS@ZIF-8 particles for HPLC. With different SOS@ZIF-8 particles prepared in this study, the selection criterion is a uniform, dense, and stable ZIF-8 nanocrystals coating on the SOS microspheres. Similar to packing the monodisperse silica spheres for HPLC, the packing of uniform ZIF-8 nanocrystals on SOS surface could produce more homogeneous porosity that may lead to higher separation efficiency.[2] As we mentioned earlier, the SOS-COOH microspheres still contained the −SH groups. The interaction of both groups with Zn^{2+} could be

DOI: 10.1021/acsami.5b04979
ACS Appl. Mater. Interfaces 2015, 7, 18054−18063

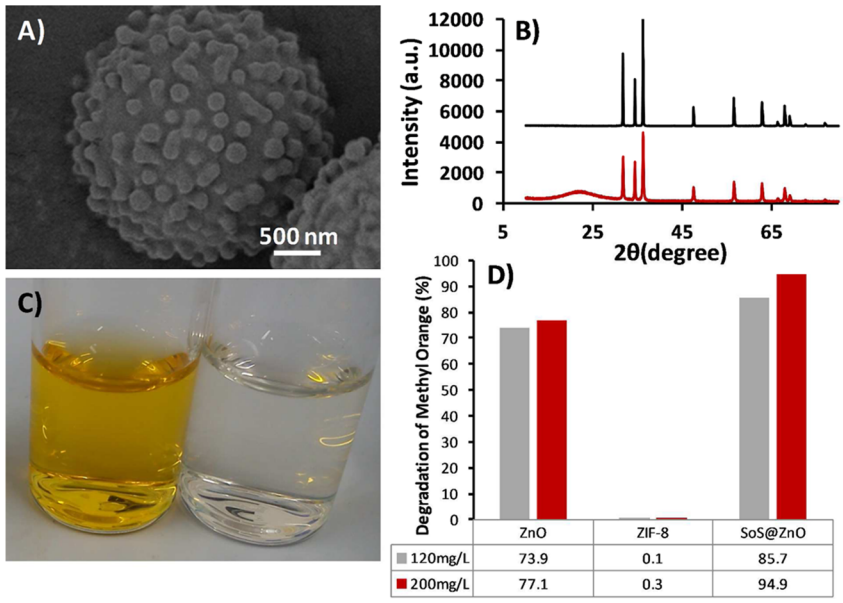

Figure 6. (A) SEM image of the SOS@ZnO microspheres created by thermally treating SOS-SH@ZIF-8 particles in air. (B) PXRD patterns of the SOS@ZnO microspheres (red line) and the ZnO particles calcined from the prepared ZIF-8 nanocrystals under the same conditions (black line). (C) Photos comparing the aqueous methyl orange solution before and after exposure to UV light at 365 nm for 4 h with SOS@ZnO microspheres. (D) Performance of ZnO nanoparticles, ZIF-8, and SOS@ZnO on degradation of methyl orange (10 mg/L in water) at room temperature over 4 h. The concentrations of catalysts are 120 and 200 mg/L, on the basis of the volume of methyl orange solution. The numbers in the table are the degradation percentages.

stronger and hence could result in stable attachment of ZIF-8 nanocrystals to the SOS surface. Thus, the SOS-COOH@ZIF-8 particles with relatively uniform and dense coating should be selected for HPLC testing.

ZIF-8 crystals contain hydrophobic micropores.[18] The columns packed with ZIF-8 particles or silica-ZIF-8 core–shell particles have been assessed for reversed-phase HPLC.[14,22] Herein, the column packed with SOS-COOH@ ZIF-8 particles (procedure 1 in H_2O, Figure S4, morphology similar to that shown in Figure 1B) was first assessed using methanol/ethanediol (99.5:0.5 v/v%) as mobile phase. However, the separation of the test mixtures (Figure S11) was poor (Figures S12 and S13). There was only a slight improvement compared to the column packed with SOS particles. This is likely the result of low loading and larger interstitial voids between the ZIF-8 nanocrystals on SOS surface. The SOS-COOH@ZIF-8 particles (prepared by procedure 2 in methanol, Figure 4D) with densely aggregated ZIF-8 nanocrystals and the overall spherical shape (for efficient packing) were then evaluated. The change of the column back pressure with the mobile phase was investigated by flushing the packed column at different flow rates. Compared to the column back pressure of the SOS-COOH particles packed column, the column back pressure was increased about 40% in the presence of ZIF-8 nanocrystals (Figure 5A). The SOS@ZIF-8 packed column generated a column pressure of 186 bar, whereas the back pressure was 132 bar for the SOS-COOH packed column at 1 mL/min. The increase in the back pressure was due to the presence of ZIF-8 nanocrystals between the nanospheres on SOS particles. However, the introduction of ZIF-8 on the surface could result in an increase in $\pi-\pi$ interaction with aromatic compounds caused by an imidazole group.[22] This was demonstrated here by separation of 1-(4-hydroxyl phenyl) ethanol, 3-[1-(methyl amino) ethyl] phenol, and 3-[1-(dimethyl amino) ethyl] phenol (Figure S11). With the SOS-COOH packed column, these aromatic compounds were not resolved and eluted as a large single peak (Figure 5B). The separation selectivity was improved with ZIF-8 nanocrystals on the SOS surface. All three aromatic compounds were resolved in less than 3 min. This separation was achieved with a flow rate of 0.35 mL/min and back pressure of 59 bar (Figure 5B). The separation of similar aromatic compounds was previously carried out using ZIF-8 particles as the stationary phase. It was found that ZIF-8 showed a good selectivity but gave inadequate mass transfer and poor chromatographic resolution.[22] Using the SOS-COOH@ZIF-8 particles as stationary phase resulted in improved chromatographic resolution and efficiency (column efficiency reaching up to 19 148 plates/m on the basis of peak 3 in Figure 5B). Another example of separation via the $\pi-\pi$ interaction mechanism was demonstrated with phenol, hydroquinone, and bibenzyl-4,4′-diol (Figure 5C). The baseline separation was achieved within 5 min at a flow rate of 0.35 mL/min. Bibenzyl-4,4′-diol showed stronger retention on the stationary phase and resulted in a retention factor of 5.7. This could be attributed to the additional $\pi-\pi$ interaction with the increase in aromaticity. Indeed, compared to the SOS-COOH column, the retention times of all these aromatic compounds are longer on the column packed with SOS-COOH@ZIF-8 particles. It is clear that the difference in $\pi-\pi$ interaction between the aromatic compounds and the coated ZIF-8 nanocrystals has led to the improved separation.

Photocatalytic Degradation of Methyl Orange. ZIF-8 nanocrystals on SOS particles were thermally decomposed in air to form a ZnO layer on the SOS microspheres, which was then evaluated for dye photodegradation. Methyl orange was chosen as a model dye because it has been used extensively in the dye industry.[23,24,32]

This study was to demonstrate the potential use of SOS@ZnO microsphere for dye photodegradation. One type of SOS@ZIF-8 composite microsphere was selected and thermally

DOI: 10.1021/acsami.5b04979
ACS Appl. Mater. Interfaces 2015, 7, 18054–18063

treated for a dye degradation test. During the thermal treatment in air at 550 °C, the organic components including the carbon chains and surface functional groups were decomposed to produce inorganic silica.[37] Therefore, the SOS surface functional groups (−COOH, −SH, and $-NH_2$) could not contribute to the degradation performance, although the surface functional groups did impact the ZIF-8 morphology. The SOS-SH@ZIF-8 composite mcirospheres (Figure 1B) were chosen because of the relatively uniform coating of small ZIF-8 nanocrystals. This could, in principle, lead to smaller ZnO nanoparticles that could have better performance for the degradation of methyl orange. The thermally treated microspheres resembled the SOS spheres (Figure 6A). The PXRD pattern showed no diffraction peaks for crystalline ZIF-8. Instead, it exhibited characteristic diffraction peaks at {100}, {002}, {101}, {102}, and {110}, indicating the hexagonal wurtzite structure of ZnO (Figure 6B).[31,32] Individual ZnO nanocrystals could not be seen on the SOS particles. Higher-resolution SEM images showed a layer of ZnO consisting of small nanograins (Figure S14). To estimate the loading of ZnO, the composite spheres (10 mg) were dissolved in 10 mL of acid solution (mixture of 0.5 M citric acid and 0.5 M HCl, with the presence of citric acid facilitating ZnO dissolution).[45] The ICP analysis gave a Zn^{2+} concentration of 77 ppm. The calculation showed a ZnO loading of 9.6 wt % in the composite microspheres.

As a control, the degradation of methyl orange was initially carried out in the presence of ZnO (20−100 nm, Figure S15) and ZIF-8 nanoparticles (synthesized with procedure 1 in water without the presence of SOS particles, Figure S8). Methyl orange with an initial concentration of 10 mg/L was used throughout this work. The degradation reaction was carried out at room temperature, and the reaction was monitored with a UV−vis spectrometer. Methyl orange exhibits strong absorption at 465 nm. A change of absorbance at 465 nm was used to monitor the dye's degradation. The experiments showed that the photodegradation did not occur in the presence of ZIF-8. As expected, the degradation of methyl orange with ZnO nanoparticles as catalyst was observed. Methyl orange was completely decomposed into colorless small molecules within 6 h.[31,32,46]

The composite SOS@ZnO particles were tested for the photodegradation of methyl organic under the same conditions (120 mg of catalyst per 1 L of methyl orange solution) as used in the control experiment. After 4 h of UV radiation at 365 nm, the yellow solution turned nearly colorless, indicating the photodegradation of methyl orange (Figure 6C). The percentage of degradation with the SOS@ZnO sphere was calculated to be 85.7% from the UV−vis data, higher than that of ZnO nanoparticles (73.9%, Figure 6D). The ZnO layer covers the SOS particles. We do not expect any adsorption of methyl orange onto the SOS particles. To confirm this, the SOS-SH particles were thermally treated in the same way (i.e., heating in air to 550 °C) and then tested for dye adsorption/degradation. There was no decrease of the concentration observed when the SOS particles were soaked in the methyl orange solution for up to 3 days. It should be noted that the commercial catalyst comprises only ZnO, whereas the loading of ZnO in the SOS@ZnO composite spheres was around 9.6%. Because the same mass of the materials was used for the photodegradation reactions, this indicated a much higher catalytic efficiency from the SOS@ZnO microspheres. A thin film of nanocrystalline ZnO was observed to cover the SOS silica microspheres. The easy access to the supported and very small ZnO nanocrystals is thought to be the reason for the superior degradation performance of the SOS@ZnO microspheres. When the concentration of the catalyst was increased to 200 mg/L, the percentage of methyl orange degradation was increased by 10%, with still no catalytic activity observed for ZIF-8 nanocrystals. However, the percentage of degradation was still higher for the SOS@ZnO composite spheres (Figure 6D). The catalytic photodegradation by SOS@ZnO particles was repeated three times. The degradation of methyl orange (>90%) was achieved in each case, with a standard deviation of <3% (Figure S16). SOS@ZnO can be readily recovered by gravimetric sedimentation or simple filtration. With spherical morphology and the micrometer sizes, these spheres may be easily packed into a column to allow continuous wastewater treatment, in a manner similar to HPLC separation.

CONCLUSIONS

SOS silica microspheres were used as support to prepare SOS@ZIF-8 composite microspheres. Uniform and dense coatings of ZIF-8 with significantly varied morphologies on the SOS particles were formed in a one-step synthesis, without the usual multiple coating procedures required. PXRD patterns confirmed the formation of crystalline ZIF-8. Although the SOS particles were nonporous, the SOS@ZIF-8 core−shell particles exhibited BET surface areas up to 500 m^2/g, attributed to the intrinsic ZIF-8 microporosity and the interstices between the shell nanoparticle. The morphology of ZIF-8 nanocrystals on SOS microspheres was strongly influenced by the silica surface functional groups (−SH, −COOH, and $-NH_2$) and precursor conditions (mainly the molar ratio of the ligand 2-MeIM to Zn^{2+}). The SOS@ZIF-8 core−shell microspheres could be easily packed into a column for HPLC separation. The ZIF-8 coating provided shell porosity and enhanced $\pi-\pi$ interaction with the aromatic compounds. This led to the fast HPLC separation of the mixtures of aromatic compounds, with column efficiency reaching up to 19 000 plates/m. Furthermore, the SOS@ZIF-8 microspheres could be transformed into SOS@ZnO upon thermal treatment in air. PXRD, SEM imaging, and ICP analysis confirmed a layer of crystalline ZnO at loading of 9.6% formed on the SOS spheres. Efficient photodegradation of methyl orange in water was demonstrated by SOS@ZnO microspheres, with easy removal of catalysts by gravimetric sedimentation and facile packing capability potentially allowing for continuous flow treatment.

ASSOCIATED CONTENT

Supporting Information

The Supporting Information is available free of charge on the ACS Publications website at DOI: 10.1021/acsami.5b04979.

Additional SEM images, PXRD data, BET data, compound chemical structures, TGA data, and dye degradation data. (PDF)

AUTHOR INFORMATION

Corresponding Author

*E-mail: zhanghf@liv.ac.uk.

Notes

The authors declare no competing financial interest.

DOI: 10.1021/acsami.5b04979
ACS Appl. Mater. Interfaces 2015, 7, 18054−18063

■ ACKNOWLEDGMENTS

We are grateful for the access to the facilities in the Centre for Materials Discovery at the University of Liverpool. J.J. acknowledges the financial support from China Scholarship Council for the academic visit to the Department of Chemistry University of Liverpool.

■ REFERENCES

(1) Yang, P.; Gai, S.; Lin, J. Functionalized Mesoporous Silica Materials for Controlled Drug Delivery. *Chem. Soc. Rev.* **2012**, *41*, 3679−3698.
(2) Hayes, R.; Ahmed, A.; Edge, T.; Zhang, H. Core−Shell Particles: Preparation, Fundamentals and Applications in High Performance Liquid Chromatography. *J. Chromatogr. A* **2014**, *1357*, 36−52.
(3) Parlett, C. M. A.; Wilson, K.; Lee, A. F. Hierarchical Porous Materials: Catalytic Applications. *Chem. Soc. Rev.* **2013**, *42*, 3876−3893.
(4) Bradshaw, D.; Garai, A.; Huo, J. Metal−Organic Framework Growth at Functional Interfaces: Thin Films and Composites for Diverse Applications. *Chem. Soc. Rev.* **2012**, *41*, 2344−2381.
(5) Banerjee, R.; Phan, A.; Wang, B.; Knobler, C.; Furukawa, H.; O'Keeffe, M.; Yaghi, O. M. High-Throughput Synthesis of Zeolitic Imidazolate Frameworks and Application to CO2 Capture. *Science* **2008**, *319*, 939−943.
(6) Park, K. S.; Ni, Z.; Cote, A. P.; Choi, J. Y.; Huang, R.; Uribe-Romo, F. J.; Chae, H. K.; O'Keeffe, M.; Yaghi, O. M. Exceptional Chemical and Thermal Stability of Zeolitic Imidazolate Frameworks. *Proc. Natl. Acad. Sci. U. S. A.* **2006**, *103*, 10186−10191.
(7) Cravillon, J.; Münzer, S.; Lohmeier, S.-J.; Feldhoff, A.; Huber, K.; Wiebcke, M. Rapid Room-Temperature Synthesis and Characterization of Nanocrystals of a Prototypical Zeolitic Imidazolate Framework. *Chem. Mater.* **2009**, *21*, 1410−1412.
(8) Pan, Y.; Liu, Y.; Zeng, G.; Zhao, L.; Lai, Z. Rapid Synthesis of Zeolitic Imidazolate Framework-8 (ZIF-8) Nanocrystals in an Aqueous System. *Chem. Commun.* **2011**, *47*, 2071−2073.
(9) Cravillon, J.; Nayuk, R.; Springer, S.; Feldhoff, A.; Huber, K.; Wiebcke, M. Controlling Zeolitic Imidazolate Framework Nano- and Microcrystal Formation: Insight into Crystal Growth by Time-Resolved In Situ Static Light Scattering. *Chem. Mater.* **2011**, *23*, 2130−2141.
(10) Wang, Y.; Xu, Y.; Ma, H.; Xu, R.; Liu, H.; Li, D.; Tian, Z. Synthesis of ZIF-8 in a Deep Eutectic Solvent Using Cooling-Induced Crystallisation. *Microporous Mesoporous Mater.* **2014**, *195*, 50−59.
(11) Bustamante, E. L.; Fernández, J. L.; Zamaro, J. M. Influence of the Solvent in the Synthesis of Zeolitic Imidazolate Framework-8 (ZIF-8) Nanocrystals at Room Temperature. *J. Colloid Interface Sci.* **2014**, *424*, 37−43.
(12) Jian, M.; Liu, B.; Liu, R.; Qu, J.; Wang, H.; Zhang, X. Water-Based Synthesis of Zeolitic Imidazolate Framework-8 with High Morphology Level at Room Temperature. *RSC Adv.* **2015**, *5*, 48433−48441.
(13) Venna, S. R.; Jasinski, J. B.; Carreon, M. A. Structural Evolution of Zeolitic Imidazolate Framework-8. *J. Am. Chem. Soc.* **2010**, *132*, 18030−18033.
(14) Fu, Y.-Y.; Yang, C.-X.; Yan, X.-P. Fabrication of ZIF-8@SiO2 Core−Shell Microspheres as the Stationary Phase for High-Performance Liquid Chromatography. *Chem. - Eur. J.* **2013**, *19*, 13484−13491.
(15) Bux, H.; Liang, F.; Li, Y.; Cravillon, J.; Wiebcke, M.; Caro, J. Zeolitic Imidazolate Framework Membrane with Molecular Sieving Properties by Microwave-Assisted Solvothermal Synthesis. *J. Am. Chem. Soc.* **2009**, *131*, 16000−16001.
(16) Cao, X.; Dai, L.; Liu, J.; Wang, L.; He, J.; Deng, L.; Lei, J. Fabrication of ZIF-8@Super-macroporous Poly(glycidyl methacrylate) Microspheres. *Inorg. Chem. Commun.* **2014**, *50*, 65−69.
(17) Pan, Y.; Lai, Z. Sharp separation of C2/C3 hydrocarbon mixtures by zeolitic imidazolate framework-8 (ZIF-8) membranes synthesized in aqueous solutions. *Chem. Commun.* **2011**, *47*, 10275−10277.
(18) Sorribas, S.; Zornoza, B.; Téllez, C.; Coronas, J. Ordered Mesoporous Silica−(ZIF-8) Core−Shell Spheres. *Chem. Commun.* **2012**, *48*, 9388−9390.
(19) Bux, H.; Feldhoff, A.; Cravillon, J.; Wiebcke, M.; Li, Y.-S.; Caro, J. Oriented Zeolitic Imidazolate Framework-8 Membrane with Sharp H_2/C_3H_8 Molecular Sieve Separation. *Chem. Mater.* **2011**, *23*, 2262−2269.
(20) Ahmed, A.; Hodgson, N.; Barrow, M.; Clowes, R.; Robertson, C. M.; Steiner, A.; McKeown, P.; Bradshaw, D.; Myers, P.; Zhang, H. Macroporous Metal−Organic Framework Microparticles with Improved Liquid Phase Separation. *J. Mater. Chem. A* **2014**, *2*, 9085−9090.
(21) Liu, S.-S.; Yang, C.-X.; Wang, S.-W.; Yan, X.-P. Metal−Organic Frameworks for Reverse-Phase High-Performance Liquid Chromatography. *Analyst* **2012**, *137*, 816−818.
(22) Centrone, A.; Santiso, E. E.; Hatton, T. A. Separation of Chemical Reaction Intermediates by Metal−Organic Frameworks. *Small* **2011**, *7*, 2356−2364.
(23) Robinson, T.; McMullan, G.; Marchant, R.; Nigam, P. Remediation of Dyes in Textile Effluent: a Critical Review on Current Treatment Technologies with a Proposed Alternative. *Bioresour. Technol.* **2001**, *77*, 247−255.
(24) Sarayu, K.; Sandhya, S. Current Technologies for Biological Treatment of Textile Wastewater−A Review. *Appl. Biochem. Biotechnol.* **2012**, *167*, 645−661.
(25) Khin, M. M.; Nair, A. S.; Babu, V. J.; Murugan, R.; Ramakrishna, S. A Review on Nanomaterials for Environmental Remediation. *Energy Environ. Sci.* **2012**, *5*, 8075−8109.
(26) Nidheesh, P. V.; Gandhimathi, R.; Ramesh, S. T. Degradation of Dyes from Aqueous Solution by Fenton Processes: A Review. *Environ. Sci. Pollut. Res.* **2013**, *20*, 2099−2132.
(27) Legrini, O.; Oliveros, E.; Braun, A. M. Photochemical Processes for Water Treatment. *Chem. Rev.* **1993**, *93*, 671−698.
(28) Paramasivam, I.; Jha, H.; Liu, N.; Schmuki, P. A Review of Photocatalysis Using Self-Organized TiO_2 Nanotubes and Other Ordered Oxide Nanostructures. *Small* **2012**, *8*, 3073−3103.
(29) Janus, M.; Morawski, A. W. New Method of Improving Photocatalytic Activity of Commercial Degussa P25 for Azo Dyes Decomposition. *Appl. Catal., B* **2007**, *75*, 118−123.
(30) Lam, S.; Sin, J.; Abdullah, A. Z.; Mohamed, A. R. Degradation of Wastewaters Containing Organic Dyes Photocatalysed by Zinc Oxide: A Review. *Desalin. Water Treat.* **2012**, *41*, 131−169.
(31) Wang, H.; Xie, C.; Zhang, W.; Cai, S.; Yang, Z.; Gui, Y. Comparison of Dye Degradation Efficiency Using ZnO Powders with Various Size Scales. *J. Hazard. Mater.* **2007**, *141*, 645−652.
(32) Kaur, J.; Bansal, S.; Singhal, S. Photocatalytic Degradation of Methyl Orange Using ZnO Nanopowders Synthesized via Thermal Decomposition of Oxalate Precursor Method. *Phys. B* **2013**, *416*, 33−38.
(33) Flores, N. M.; Pal, U.; Galeazzi, R.; Sandoval, A. Effects of Morphology, Surface Area, and Defect Content on the Photocatalytic Dye Degradation Performance of ZnO Nanostructures. *RSC Adv.* **2014**, *4*, 41099−41110.
(34) Du, Y.; Chen, R. Z.; Yao, J. F.; Wang, H. T. Facile Fabrication of Porous ZnO by Thermal Treatment of Zeolitic Imidazolate Framework-8 and Its Photocatalytic Activity. *J. Alloys Compd.* **2013**, *551*, 125−130.
(35) Wu, R.; Wang, D. P.; Han, J.; Liu, H.; Zhou, K.; Huang, Y.; Xu, R.; Wei, J.; Chen, X.; Chen, Z. A General Approach Towards Multi-Faceted Hollow Oxide Composites Using Zeolitic Imidazolate Frameworks. *Nanoscale* **2015**, *7*, 965−974.
(36) Cao, X.; Zheng, B.; Rui, X.; Shi, W.; Yan, Q.; Zhang, H. Metal Oxide-Coated Three-Dimensional Graphene Prepared by the Use of Metal−Organic Frameworks as Precursors. *Angew. Chem.* **2014**, *126*, 1428−1433.
(37) Ahmed, A.; Ritchie, H.; Myers, P.; Zhang, H. One-Pot Synthesis of Spheres-on-Sphere Silica Particles from a Single Precursor for Fast HPLC with Low Back Pressure. *Adv. Mater.* **2012**, *24*, 6042−6048.

DOI: 10.1021/acsami.5b04979
ACS Appl. Mater. Interfaces 2015, 7, 18054−18063

(38) Ahmed, A.; Abdelmagid, W.; Ritchie, H.; Myers, P.; Zhang, H. Investigation on Synthesis of Spheres-on-Sphere Silica Particles and Their Assessment for High Performance Liquid Chromatography Applications. *J. Chromatogr. A* **2012**, *1270*, 194−203.
(39) Hayes, R.; Myers, P.; Edge, T.; Zhang, H. Monodisperse Sphere-on-Sphere Silica Particles for Fast HPLC Separation of Peptides and Proteins. *Analyst* **2014**, *139*, 5674−5677.
(40) Ahmed, A.; Forster, M.; Clowes, R.; Bradshaw, D.; Myers, P.; Zhang, H. Silica SOS@HKUST-1 Composite Microspheres as Easily Packed Stationary Phases for Fast Separation. *J. Mater. Chem. A* **2013**, *1*, 3276−3286.
(41) Brown, J.; Mercier, L.; Pinnavaia, T. J. Selective Adsorption of Hg^{2+} by Thiol-Functionalized Nanoporous Silica. *Chem. Commun.* **1999**, 69−70.
(42) Li, G.; Zhao, Z.; Liu, J.; Jiang, G. Effective Heavy Metal Removal from Aqueous Systems by Thiol Tunctionalized Magnetic Mesoporous Silica. *J. Hazard. Mater.* **2011**, *192*, 277−283.
(43) Lu, G.; Li, S.; Guo, Z.; Farha, O. K.; Hauser, B. G.; Qi, X.; Wang, Y.; Wang, X.; Han, S.; Liu, X.; DuChene, J. S.; Zhang, H.; Zhang, Q.; Chen, X.; Ma, J.; Loo, S. C. J.; Wei, W. D.; Yang, Y.; Hupp, J. T.; Huo, F. Imparting Functionality to a Metal−Organic Framework Material by Controlled Nanoparticle Encapsulation. *Nat. Chem.* **2012**, *4*, 310−316.
(44) Choi, K.-S. Shape Control of Inorganic Materials via Electrodeposition. *Dalton Trans.* **2008**, 5432−5438.
(45) Mudunkotuwa, I. A.; Rupasinghe, T.; Wu, C.; Grassian, V. H. Dissolution of ZnO Nanoparticles at Circumneutral pH: A Study of Size Effects in the Presence and Absence of Citric Acid. *Langmuir* **2012**, *28*, 396−403.
(46) Baiocchi, C.; Brussino, M. C.; Pramauro, E.; Prevot, A. B.; Palmisano, L.; Marcì, G. Characterization of Methyl Orange and its Photocatalytic Degradation Products by HPLC/UV−VIS Diode Array and Atmospheric Pressure Ionization Quadrupole Ion Trap Mass Spectrometry. *Int. J. Mass Spectrom.* **2002**, *214*, 247−256.

DOI: 10.1021/acsami.5b04979
ACS Appl. Mater. Interfaces 2015, 7, 18054−18063